Jour. Fac. Sci., Hokkaido Univ., Ser. VII (Geophysics), Vol. 10, No. 1, 135-153, 1996.

Evolution Process and Precipitation Particles of an Isolated Echo Observed with Dual-Polarization Doppler Radar near Sapporo on July 9, 1992

Nobuhiro Takahashi*, Hiroshi Uyeda and Katsuhiro Kikuchi

Division of Earth and Planetary Sciences, Graduate School of Science, Hokkaido University, Sapporo 060, Japan

(Received November 17, 1995)

Abstract

An isolated summer convective cloud, which was observed near Sapporo by an X-band dual-polarization Doppler radar on July 9, 1992, was alalyzed from the viewpoints of cloud physic and kinematics. The life stages of the early development stage, the rapid development stage, and the mature to decaying stage were analyzed using the data from three RHI scans. The ice containing region was determined by using Z_H (horizontally polarized reflectivity) and *ZDP* (reflectivity difference). At the rain region, the raindrop size distribution was deduced from an analysis of the Z_H and Z_{DR} (differential reflectivity factor), assuming an exponential drop size distribution (DSD). Kinematic analysis was performed using Doppler velocity data.

At the early development stage, the echo showed a high Z_{DR} value with a moderate Z_H indicating that the echo consisted of large raindrops with low number concentration. The kinematic field showed weak convections within the echo. At the next stage (rapid development stage), the echo developed rapidly, and an ice region appeared above the environmental 0°C level. The DSD of the rain region indicated that large raindrops still existed at the lower altitudes (<2 km) and smaller raindrops with larger number concentration appeared above it. After the echo reached the mature to decaying stage, the region of the large raindrops with low number concentration disappeared. These results indicate that different DSD clearly appeared during the life cycle of the echo.

This study indicates that the combination of polarimetric data and Doppler velocity data is useful for understanding the cloud development processes and that polarimetric data is helpful when estimating the rainfall intensity corresponding to the cloud development stage.

* Present affiliation: Communications Research Laboratory, Kashima, Ibaraki Pref. 314.

1. Introduction

Recent progress in the development of dual-polarization radar had enabled researches to infer the cloud physical properties such as the hydrometeor types and rainfall rate estimation. Seliga and Bringi (1976) first proposed the usage of polarization parameters. The major parameters derived from dual-polarization radar are the differential reflectivity factor Z_{DR}, the linear depolarization ratio LDR, the correlation coefficient between the horizontal and vertical polarized wave ρ_{hv}, and the specific differential phase K_{DP}. A comprehensive explanation of these parameters is described by Zrnic' (1991). To determine the hydrometeor type, Z_H and Z_{DR} are utilized. In addition, the parameter *ZDP* (reflectivity difference; Meischner et al., 1991) is also used to discriminate between ice and rain. The LDR and ρ_{hv} are utilized to detect the mixed phase layers such as the bright band (Zrnic' et al., 1993a; Zrnic' et al., 1993b). The K_{DP} is good for measuring the rainfall rate (Sachidananda and Zrnic', 1987; Balakrishnan and Zrnic', 1990).

At the rain region, the drop size distribution (DSD) is estimated under a assumption that a drop's shape changes with size (e.g. Illingworth, 1992). The estimation procedure is explained in the next section. However, discriminations of ice crystals, snow and graupel and the estimation of size distribution are difficult in the ice region, because shape is no longer a systematic function of the size or types of hydrometeors.

Kinematics in a cloud are detected by a Doppler radar (Doviak and Zrnic', 1984). Therefore the combination of a dual-polarization radar and a Doppler radar can be used to determine how the cloud development process is related to the clound physical processes. Conway and Zrnic' (1993) used a multiparameter radar and a dual Doppler radar for deducing the growth process of hail along its trajectory which was obtained by a dual Doppler wind field. Zrnic' et al. (1993b) described a hydrometeors distribution in a hail storm using a dual-polarization radar and a Doppler radar. They were able to deduce self-consistent hydrometeor distribution in a hail storm without direct measurement. This analysis procedure would be applicable to the study of DSD of rain in other convective clouds, if both dual-polarization and Doppler radar data are available at the same time.

In this study, the cloud physical and kinematic processes of an isolated cloud that was observed near Sapporo, Hokkaido, Japan on July 9, 1992, using a Hokkaido University X-band dual-polarization Doppler radar, are analyzed. The cloud physical information was derived from a dual-polarization radar and

the kinematic information was derived from Doppler velocity data. Because of the limitation of the radar's function, the parameters Z_H, Z_{DR}, and ZDP were utilized for the cloud physical analysis. The analyses were mainly for discrimination between the ice region and rain region and estimation of DSD at the rain region. The development process of the cloud was described using Doppler velocity fields.

2. Radar measurements of hydrometeors

The radar specifications are shown in Table 1. The radar has two observation modes: one is Doppler mode, and the other is dual-polarization mode. The Doppler mode collects the reflectivity data, the Doppler velocity, and the spectrum width of the Doppler velocity with a range resolution of 250 m for a 60 km observation range. The dual-polarization mode collects data on polarimetric reflectivity; the combination of the incidental polarization (horizontal or vertical) and the received polarization (horizontal or vertical). In this observation, reflectivity that is transmitted and received by horizontal polarization (horizontally polarized reflectivity factor, Z_H) and transmitted and received by vertical polarization (vertically polarized reflectivity, Z_V) is collected with a range resolution of 125 m for a 30 km observation range. The transmitting polarization was switched from pulse to pulse. Observed pulse data was integrated within a box area of RHI scan of 1 km (horizontal)$\times$0.5 km (vertical)

Table 1. The specification of Hokkaido University Dual-Polarization Doppler Radar

Parameter	Dual Polarization	Doppler
Wave length (cm)	3.2	3.2
Maximum range (km)	31.5	63.5
Nyquist velocity (m/s)	–	±12.0
Pulse duration (μs)	0.8	0.4
Pulse repetition frequency (Hz)	750	1,500
Azimuthal resolution (deg.)	0.35	0.7
Beam width (deg.)	2.0	2.0
Number of samples	254	254
Gete spacing (m)	62.5	62.5
Sample spacing (m)	125	250
Antenna rotation (rpm)	4	1
Antenna diameter (m)	1.2	1.2

containing more than 250 pulse hits.

Observations were made at 10 or 15 minute intervals by several PPI (Plan Position Indicator) and RHI (Range Height Indicator) scans in the Doppler mode; the dual-polarization mode was selected only for the RHI scans, which were set at the same azimuth as those in the Doppler RHI mode. In order to investigate the vertical development of a convective cloud, the dual-polarization data and Doppler velocity data of an RHI scan are required to be collected at the same azimuth and at the same time. However, it takes 60 to 80 seconds to perform both observation modes of the RHI scan, so the time difference between the cloud physical and kinematic observation is about one minute. Because of the limited observation range (30 km, see Table 1) in the dual-polarization mode, only 3 RHI scans for both the dual-polarization and Doppler radar data (1005, 1013, and 1026JST on July 9, 1992; JST=UTC+9 hours) are available for the comparison.

For dual-polarization data analysis, the differential reflectivity factor Z_{DR} which can provide hydrometeor shape information and the reflectivity difference ZDP were utilized. The differential reflectivity factor Z_{DR} is defined as,

$$Z_{DR}=10\log\,(Z_H/Z_V) \tag{1},$$

and ZDP is defined as,

$$ZDP=10\log\,(Z_H-Z_V) \tag{2}.$$

From Seliga and Bringi (1976), the relationship between DSD and the reflectivity factors of horizontal and vertical polarization are expressed as

$$Z_H=\int_0^\infty D^6\left|\frac{m^2-1}{4\pi+(m^2-1)P'}\right|^2 N(D)dD \tag{3}$$

$$Z_V=\int_0^\infty D^6\left|\frac{m^2-1}{4\pi+(m^2-1)P}\right|^2 N(D)dD \tag{4}$$

respectively, where D is the raindrop diameter of equivalent volume sphere, $N(D)$ is the number concentration of drop size D, m is the refractive index of water, and $P(P')$ is a kind of shape factor of a raindrop. $P(P')$ is expressed as

$$P=\frac{4\pi}{e^2}\left[\,1-\left(\frac{1-e^2}{e^2}\right)^{\frac{1}{2}}\arcsin(e)\right] \tag{5}$$

$$P'=2\pi-P/2 \tag{6}$$

where e is eccentricity $e=\frac{(b^2-a^2)^{\frac{1}{2}}}{b}$ (a and b are the short and long axis lengths, respectively). The shape of a raindrop depends on its size; as the size increases the droplet becomes oblate (smaller droplets have a spherical shape).

In this study, the experimental relationship between axis ratio and diameter of an equivalent sphere by Pruppacher and Beard (1970) are used for the calculation;

$$a/b=[1-(9/16)a_0\rho V_t^2/S] \quad (140\ \mu\mathrm{m}<a_0<500\ \mu\mathrm{m}) \tag{7}$$

$$a/b=1.030-0.124a_0 \quad (500\ \mu\mathrm{m}<a_0<4.5\ \mathrm{mm}) \tag{8}$$

where a_0 is the radius of the equivalent sphere, ρ is the saturated air density, Vt is the terminal fall velocity, and S is the surface tension of water at 20°C.

If both Z_H and Z_{DR} are measured for rain, we can derive the two-parameter DSD. Therefore, in this case study, an exponential raindrop spectrum (Illingworth and Caylor, 1989) of the form:

$$N(D)=N_0\exp(-3.67D/D_0)\ (\mathrm{m^{-3}\,mm^{-1}}) \tag{9}$$

where, D_0 is the equivolumetric diameter (mm), is assumed to be fitted (Illingworth, 1992). By substituting equation (9) for $N(D)$ in equations (3) and (4), the values of Z_H and Z_{DR} are calculated as a function of D_0 and N_0. Then, by using observed Z_H and Z_{DR}, the most suitable values of N_0 and D_0 are estimated (Illingworth, 1992).

To hydrometeors other than rain, for example snow and graupel, this relationship could not be applied, since the shape of an ice particle is not parameterized by its size. The Z_{DR} value of graupel generally ranges from 1 dB to a nagative value, and that of snow ranges from 1 dB to 0 dB (Illingworth and Caylor, 1991; Hall et al., 1984). A wider range of Z_{DR} values could be observed for snow as Uyeda et al. (1991) reported a large value of Z_{DR} (>1 dB) near the echo tops of snow clouds. The ZDP value is also a useful indicator for the discrimination of an ice region. Golestani et al. (1989) showed that a unique relationship (linear on a log-log scale) exists between ZDP and Z_H in rain having a gamma size distribution. Deviations from this relationship are attributed to ice hydrometeors and can be used to obtain the fraction of Z^H contributed by ice within the resolution volume. The relationship between ZDP (in decibel) and Z_H (in decibel) was $ZDP=1.2Z_H-15.8$ from Golestani et al. (1989). Conway and Zrnic' (1993) obtained the relationship $ZDP=1.13Z_H-9.1$ from their observation (see their Fig. 5). In this case study, the relationship was $ZDP=1.07Z_H-6.2$, this relationship was calculated from three RHI scan data used in this analysis. The deviation of Z_H from the fitted relationship is shown as $Z_H{}^{\mathrm{I}}$ ($Z_H{}^{\mathrm{I}}=Z_H-(ZDP+6.2)/1.07$; see Golestani et al., 1989, and Conway and Zrnic', 1993). In this study, the positive region of $Z_H{}^{\mathrm{I}}$ is used as an indicator for the existence of ice (sign of ice existence).

Analysis was first performed to discriminate between the ice containing region and the rain region. After that, N_0 and D_0 were calculated from Z_H and Z_{DR} by assuming the exponential DSD, in the rain region. Also, the rainfall intensity was calculated from DSD.

Doppler mode data were utilized to infer the vertical circulation of the cloud. If the cloud has two dimensional or axisymmetric structure, vertical circulation is deduced by the integration of radial divergence of Doppler velocity in RHI plane. In this case, we assumed that the target echo had relatively simple structure, especially at the early stage of the echo. However, as far as the echo does not have ideal structure, quantitative estimation of vertical motion is impossible with single Doppler radar. Therefore, we only estimated updraft region and downdraft region from Doppler velocity field in RHI plane.

In this study, the development process of the echo was inferred from the strength of the reflectivity, echo top height and wind field derived from the Doppler velocity. The cloud physical characteristics were inferred by the dual-polarization radar data.

3. Results

3.1 Environmental condition

The location of the radar in this case is shown in Fig. 1. The first echo of the target cloud was observed about 20 km south of the radar location at 1000JST, July 9, 1992 as shown in Fig. 1. The synoptic condition about one hour before the echo initiation (09JST on July 9, 1992) of this case is shown in Fig. 2. The surface weather map shows that a low pressure system located over Hokkaido Island. Therefore a warm southwesterly advection occurred in this area. At the 500 hPa surface, a cold trough center (−18°C) located over Hokkaido Island decreased static stability. Vertical profiles of the potential temperature (θ), equivalent potential temperature (θ_e), and saturated equivalent potential temperature (θ_e*) are shown in Fig. 3. Under the influence of the 500 hPa cold advection, the layer below 3 km was convectively unstable. The layer from 3 km to 6 km was neutral with a relatively dry air, and stable layer existed above 6 km. The convective available potential energy (CAPE) calculated from this sounding was 960 J/kg. If we employ the surface temperature at 10JST instead of the 09JST sounding, the value rises to 1,800 J/kg. Under these conditions, a tornado-producing hail storm developed (not shown in this paper) in the radar observation range. The target echo did not produce hail or a tornado, but developed moderately.

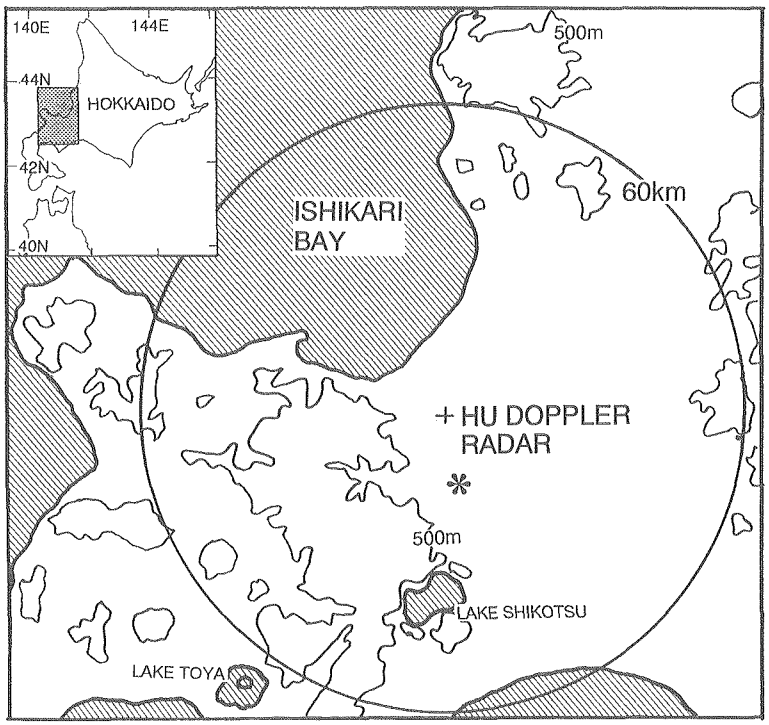

Fig. 1. Map of the observation area. The location of the Hokkaido University dual-polarization Doppler radar and its 60 km range are depicted as a cross and circle, respectively. The symbol (*) indicates the location of the first echo.

3.2. *Radar analyses*

Fig. 4 shows the transition of the target echo of PPI scans (elevation angle= 3°). This radar echo consisted of two convective cells. At the earlier time (~1041JST), a northeastern cell dominated the echo. This cell reached its maximum reflectivity at 1010JST, after that, the echo intensity became weaker. The other cell, which was located at the southwestern part of the echo, became stronger and it dominated the echo after 1041JST. The echo moved east, and was out of the observation range at 1113JST. Since, dual-polarization analysis was available within a 30 km range as mentioned in chapter 2, the analysis of the northern echo cell from tre developing stage to the mature and decaying stage will be shown in the following paragraphs.

In order to understand the life cycle of this echo cell, the vertical cross section of the northern echo cell was examined. Figure 5 shows the vertical

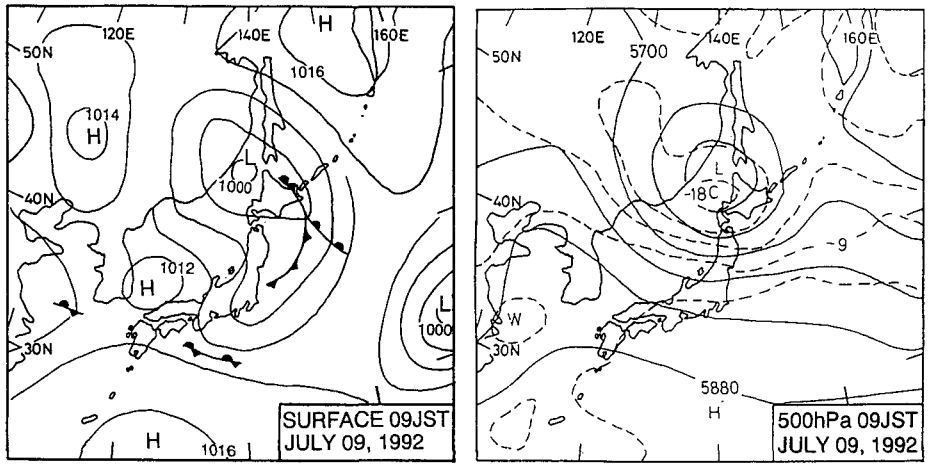

Fig. 2. Surface and 500 hPa weather charts at 09JST on July 9, 1992. In the 500 hPa chart, the solid and dashed lines indicate the isopleth of height (m) and temperature (°C).

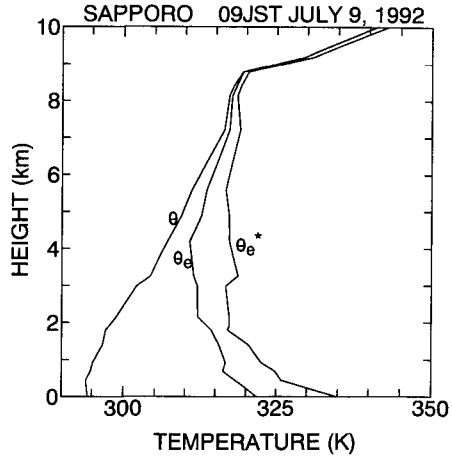

Fig. 3. Vertical profiles of potential temperature, equivalent potential temperature, and saturated equivalent potential temperature at 09JST on July 9, 1992.

cross section of the Z_H superimposed positive Z_H' region, Z_{DR}, and Doppler velocity field of RHI scans.

At 1005JST, the echo exhibited a relatively weak Z_H with a low echo top height of 5 km (2 km above the environmental melting level). A maximum Z_H (35 dBZ) core existed between 2 and 3 km levels. At this time, the echo did not

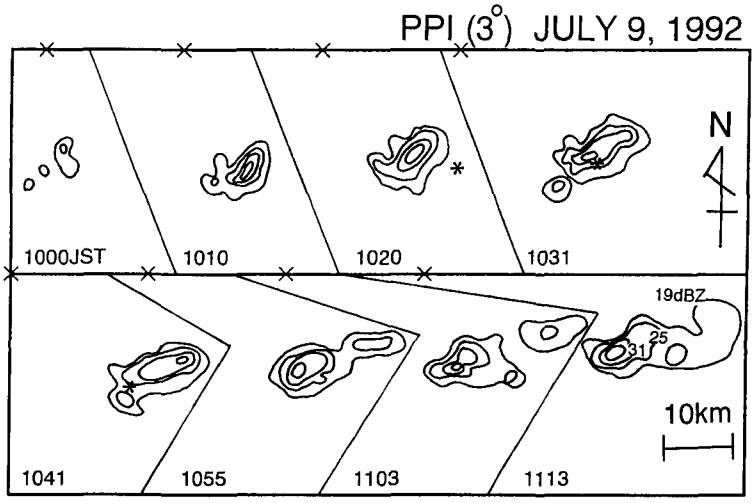

Fig. 4. Transition of PPI scan radar echoes (elevation=3°) from 1000JST to 1113JST on July 9, 1992. Contour interval is 6 dB from 19 dBZ. The symbol (×) indicates the relative position of the radar site. Also, the locations of Eniwa- Shimamatsu relative to the echo at 1020JST, 1031JST, and 1041JST are indicated by the symbol (*).

reached to the ground. On the other hand, the Z_{DR} shows a large value (greater than 2 dB with a maximum value of 5 dB) and a large Z_{DR} region coincided with the strong Z_H region.

The maximum Z_{DR} was extremely large requiring a drop diameter of about 6 mm for the mono disperse distribution, but we could not determine whether it came from the radar system bias or a meteorological phenomena. Illingworth et al. (1987) observed an extremely large Z_{DR} (4.1 dB) where reflectivity Z is less than 30 dBZ and they concluded that there was the possibility of large drops (5 ~6 mm in diameter) with a low number concentration. However, we should consider that our value contains some system bias due to the differences of system loss between horizontal and vertical polarization channel. However, it was not estimated correctly because there were no reference data except only one surface rainfall data. Therefore, we used original Z_{DR} data for the calculation of the DSD, even though the Z_{DR} values are somewhat large. At this time positive $Z_H{}^i$ did not appear in the echo suggesting the absence of ice. Doppler velocity field shows scattering pattern of updraft and downdraft, but updraft region is much larger than downdraft region.

Rapid development occurred at 1013JST and reached maximum Z_H (>35

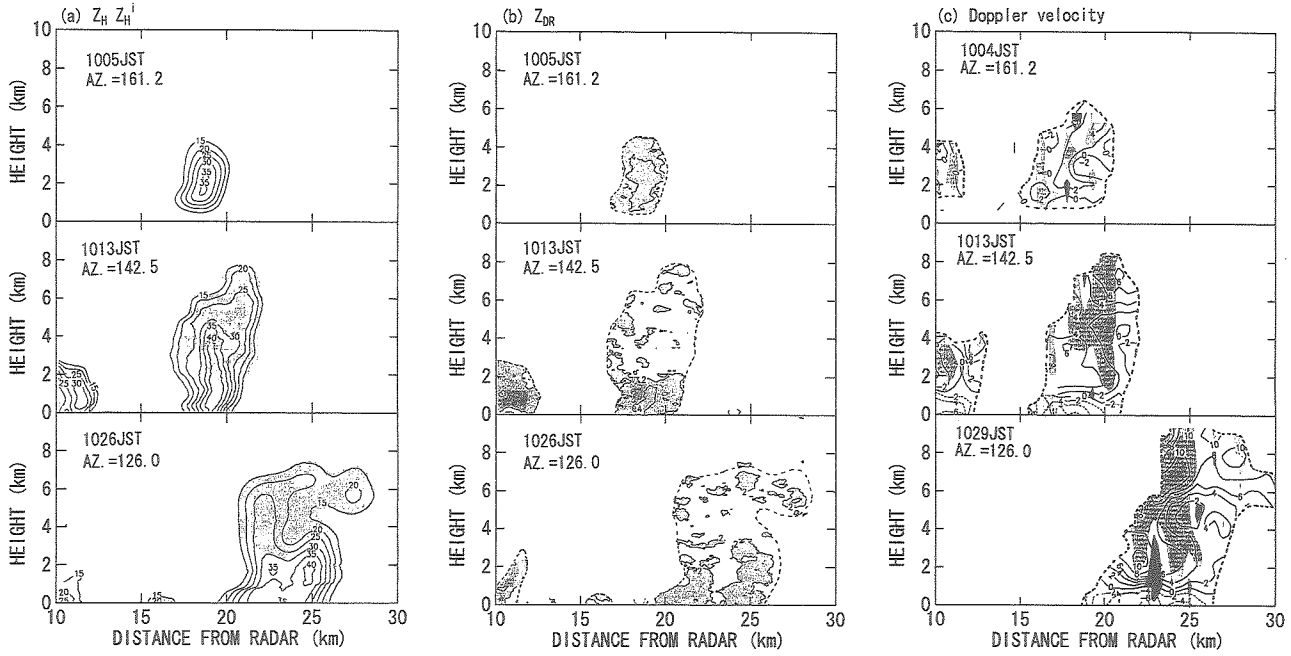

Fig. 5. Vertical cross sections of reflectivity with positive Z_H^i (shaded), Z_{DR} and Doppler velocity at 1005JST, 1013JST, and 1026JST on July 9, 1991. Contour interval of reflectivity is 5 dB from 15 dBZ, of Z_{DR} is 1 dB, and of Doppler velocity is 2 m/s (positive value indicates receding component); Z_{DR} greater than 2 dB is stippled. In Doppler velocity frames, stippled region indicates the updraft region and darkened region indicates the downdraft region.

dBZ) but the height of the maximum Z_H core descended to below 2 km and reached to the ground. Positive $Z_H{}^i$ occupied the altitudes above 2 or 3 km, suggesting the existence of ice above the melting level (about 3 km in height). Large Z_{DR} values (>2 dB) remained at the lower altitudes (<2 km) coinciding with the strong Z_H region; on the other hand, small Z_{DR} values (<2 dB) existed at the altitudes above 2 km. The region where Z_{DR} is greater than 4 dB still exited at this stage. At this time, Doppler velocity field shows convergence which is similar to 1005JST echo except divergent flow below 1 km in height. This Doppler velocity field suggests that updraft region occupied the echo above 2 km, but downdraft appeared in the lower altitude coinciding with the large Z_{DR} and strong Z_H region.

At 1026JST, the Z_H became weaker and the strong Z_H region descended (compare the height of the 30 dBZ region at 1031JST and 1026JST) and the positive $Z_H{}^i$ region located above 3 km. At this time, the echo formed an anvil

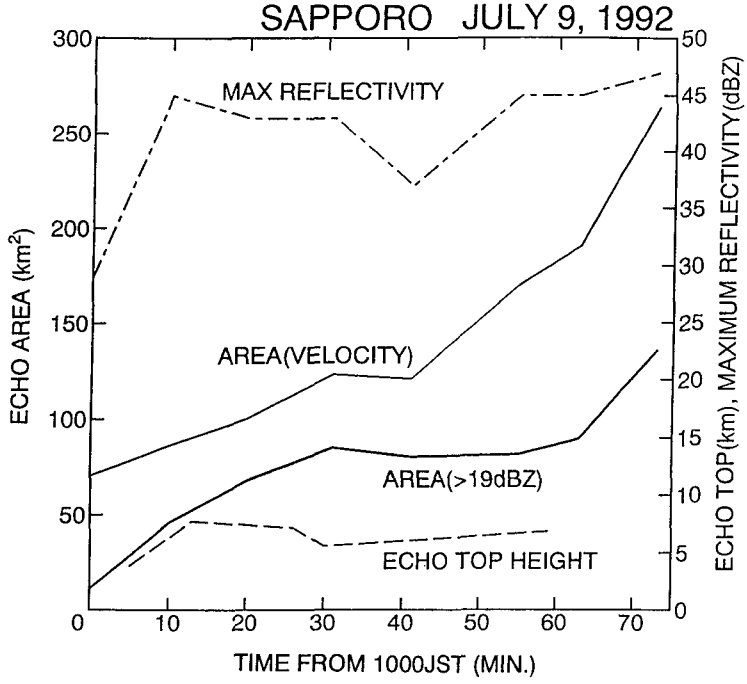

Fig. 6. Temporal variations in echo areas where Doppler velocities were detectable (thin solid line) and where reflectivities were greater than 19 dBZ (bold solid line), echo top height (dashed line), and maximum reflectivity (dash dot line) from 1000JST, July 9, 1992.

cloud. The larger Z_{DR} region (4 dB) which was seen at 1005JST and 1013JST also decayed at 1026JST. The Z_{DR} value at the strong echo region of the lower altitude was around 2 dB. Doppler velocity field shows that the updraft region still occupied above 2 km, while distinct downdraft appeared below 3 km.

The life cycle of this echo is summarized in Fig. 6, which expresses the temporal variation of the echo area, the echo top height, and the maximum Z_H. The maximum Z_H graph shows two maxima (at 10 minutes and 73 minutes in Fig. 6), coinciding with each of the echo cells mentioned in Fig. 4. The earlier echo cell (northeastern echo cell in Fig. 4) dominated the area from 1000JST to 1040JST (0 to 40 minutes in Fig. 6) and after that a newly developed echo cell dominated the echo area, as shown in Fig. 4. Therefore, the earlier maximum (1010JST) coincided with the earlier stage of the northeastern cell in Fig. 4. The echo top height rapidly increased between the early development stage (1005JST) and rapid development stage (1013JST), and reached to the maximum height. This maximum Z_H appeared about 5 minutes before the echo reached the maximum height, indicating that the maximum Z_H region formed before the echo reached the maximum (vertical) development. The echo area constantly increased in Fig. 6, this was partly caused by the broadening of the earlier echo cell and partly caused by the development of the second echo cell.

Figure 7 shows a scatter plot of Z_H and average Z_{DR} at the Z_H core (central) region for 3 RHI frames. Each point comes from 0.5 km$\times$0.5 km squares (66 data points) sampled in the RHI frames; numbers indicate the height of each squares. In the each square, the average Z_{DR} was calculated for the same Z_H (2 dB step). At 1005JST, the Z_{DR} values were much higher than those of the Marshall-Palmer (M-P) distribution for the same Z_H from a height of 0.5 km to 4 km. High Z_{DR} appeared at the altitudes between 1.5 and 3.0 km. At this time, the Z_{DR} value was almost proportional to the Z_H value. At 1013JST, the Z_H-Z_{DR} relationship at 0.5, 1.0, and 1.5 km were similar to those at altitudes from 1.5 to 3.0 km at 1005JST. On the other hand, the values were close to the M-P distribution at the higher altitudes. This characteristic of the higher altitude at 1013JST extended entirely from the surface to the 0°C level at 1026JST.

The relationship between N_0 and D_0 calculated from the Z_H and Z_{DR} data in Fig. 7 is shown in Fig. 8. The DSD of the early stage (1005JST) shows the low number concentration of large drop size (D_0 ranges from 2 mm to 3.7 mm). A highly variable number concentration at 1013JST appeared at 1013JST, when it varied from 10 to 10,000. Figure 9 demonstrates that the number concentration increased with the height. Furthermore, an apparent change in the number

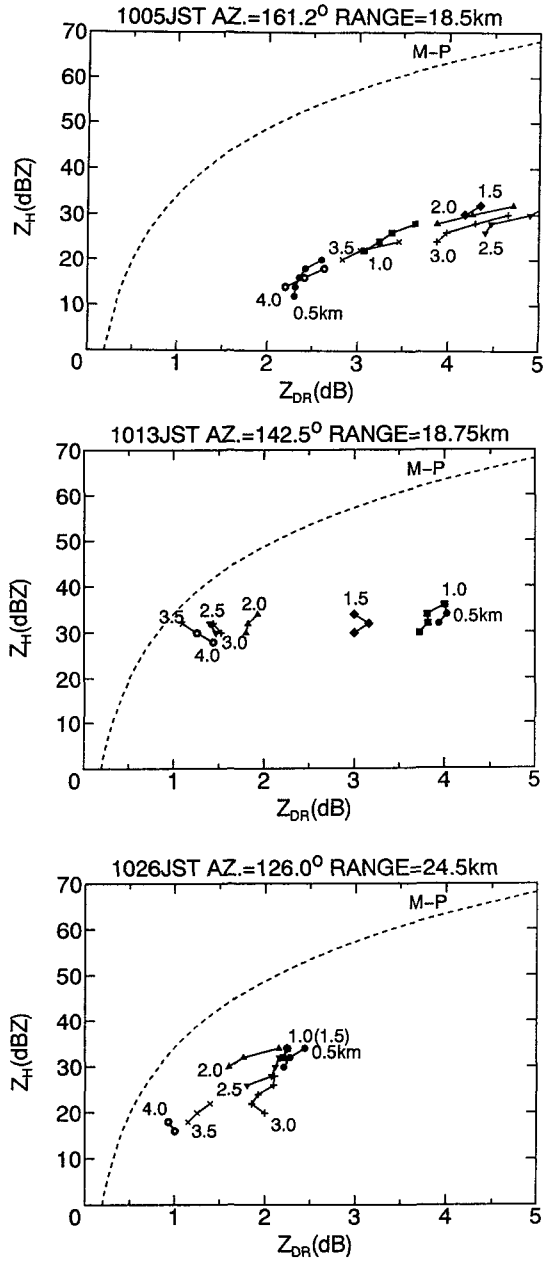

Fig. 7. Relationships between Z_{DR} and Z_H at the core region of the echo from 0.5 km to 4.0 km in height for three RHI scans at 1005JST, 1013JST, and 1026JST. Data was sampled in 0.5 km×0.5 km area (66 data points). Numbers in the figure express the height. Dashed curve indicates the relationship for the Marshall-Palmer distribution.

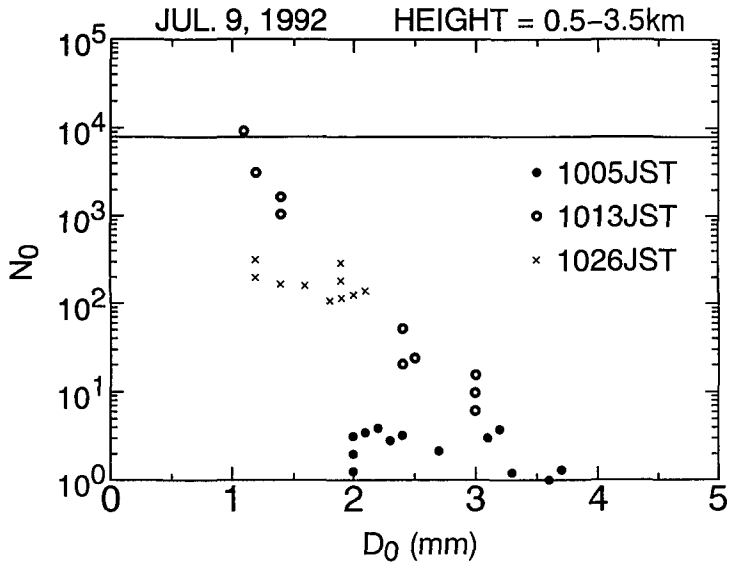

Fig. 8. Values of N_0 and D_0 for the Z and Z_{DR} data in Fig. 7. The horizontal solid line is for a Marshall-Palmer distribution ($N_0 = 8{,}000\ m^{-3}\ mm^{-1}$).

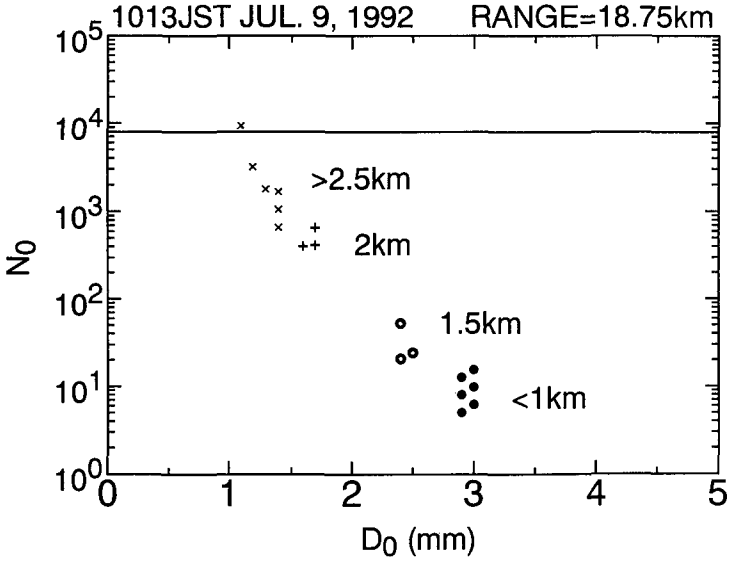

Fig. 9. Values of N_0 and D_0 for the Z and Z_{DR} data of 1013JST at the heights <1 km, 1.5 km, 2.0 km, and >2.5 km.

Table 2. Characteristics of DSD, Doppler Velocity field, and Z_H^i for each stage.

stage / parameter	early development stage	rapid development stage		mature to dissipating stage	
DSD	large D_0 small N_0	large D_0 small N_0 (<2 km)	small D_0 large N_0 (>2 km)	small D_0 large N_0	
Doppler velocity field below 4 km	convergence	convergence		convergence (>2 km)	divergence (<2 km)
region of $Z_H^i>0$	None	>3 km		>3 km	

concentration appeared at altitudes between 1.5 km and 2 km. The DSD below 1.5 km was similar to that of 1005JST but with slightly smaller D_0 and higher N_0. At 1026JST (Fig. 8), the DSD was relatively small D_0 and large N_0 which was similar to the DSD appeared above 2 km in height in the 1013JST echo.

In order to check the observed Z_H and Z_{DR} values, radar estimated rainfall amount was roughly compaped with the surface observation at an AMeDAS station (Eniwa-Shimamatsu; marked as "*" in Fig. 4). The rainfall intensity was calculated by using the DSD calculated from Z_H and Z_{DR} and an empirical formula for the terminal fall velocity of the raindrops. The rainfall amount at Eniwa-Shimamatsu was 4 mm from 10JST to 11JST. The echo transition suggested that it took the echo about 20 minutes to pass over Eniwa-Shimamatsu (from 1028 to 1048JST). Therefore a rainfall intensity was estimated to be about 12 mm/h. On the other hand, from the Z_H and Z_{DR} relationship of the 1026JST echo, the rainfall intensity was calculated to be about 4 to 5 mm/h. This difference might be caused by under estimation of the reflectivity data and/or over estimation of the Z_{DR}. The effect of the underestimation of Z_H and over estimation of Z_{DR} on D_0 and N_0 will be discussed in section 4.2. Another reason for this difference was that the 1026JST data did not represent the rainfall over Eniwa-Shimamatsu. As seen in Fig. 4, strong echo region passed over Eniwa-Shimamatsu after, 1031JST.

4. Discussion

4.1. Relationship between echo evolution and drop size distribution

The changes in DSD will be discussed in this subsection from the viewpoint of vertical circulation explained in Fig. 5. The DSD at 1005JST and lower altitudes (<1.5 km) at 1013JST was characterized as large drops with low number concentrations. At 1005JST, updraft region sparsely existed in the

echo, while distinct updraft region did not appeared below 2 km at 1013JST.

On the other hand, high number concentration of relatively small particles appeared above 2 km at 1013JST and below 3 km (whole rain region) at 1026JST. As mentioned above, updraft region occupied above 2 km and it reached a height of about 8 km at 1013JST and 1026JST. In addition, apparent down draft appeared at 1026JST. This result suggests that the strong updraft played important role to characterize the DSD. Generally, large raindrops which have enough fall speed to overcome the updraft speed can fall below the updraft region which well explain the observed DSDs in the echo at 1013JST and 1026JST. Since strong updraft existed above 2 km in height at 1013JST, only large raindrops appeared below it. At 1026JST, low level divergent flow (indicating downdraft at this height) dominated below 3 km in height and small raindrops increased below 2 km.

On the basis of the radar analyses, we infer the cloud development process as follows: The echo formed mainly below the melting level in the early stages (the 0°C level in this case was at altitudes of about 3.0 km) and the 1005JST echo was observed several minutes after the first echo. This suggests the possibility of warm rain (collision and coalescence) process worked in the echo during the earlier stages. This result indicates the possibility to produce large few raindrops through warm rain process, although the raindrops of warm rain clouds are generally small as reported by Takahashi et al. (1989).

As the updraft became stronger, the echo rapidly extended vertically far above the melting level at 1013JST, which suggests that raindrops were produced through the cold rain indicating the production of relatively large raindrops through the melting of snow flakes, however, estimated DSD from Z_H and Z_{DR} was smaller than the DSD of the early stage (note that the DSD indicates that the echo consisted of larger raindrops compared with the Marshall-Palmer DSD). The $Z_H{}^i$ in Fig. 5 also indicates the existence of ice above the melting level. However, there is no evidence to confirm this scenario, and this discussion only expresses a possible mechanism for raindrop formation. If we only use dual-polarization radar, more parameters are needed to infer microphysical structures in clouds.

4.2 Accuracy of rainfall estimation

In chapter 3, the estimated rainfall intensity (5 mm/h) was much lower than the surface observation (12 mm/h) if the echo at 1026JST caused the rainfall at Eniwa-Shimamatsu. One possible reason for that is that the reflectivity or differential reflectivity factor were biased. In this subsection, we roughly

estimated the possible DSD which is consistent with the surface observed rainfall rate.

For the same Z_{DR} (for example 2 dB), a 4 dB increase in Z_H (from 37 dBZ to 41 dBZ) induces that rainfall intensity increases from 5 mm/h to 10 mm/h. For the same Z_H (for example 40 dBZ), a 0.5 dB reduction of Z_{DR} (e.g., 2 dB to 1.5 dB) changes the rainfall intensity from 5 mm/h to 15 mm/h. Therefore, underestimation of the rainfall intensity might be caused by a bias of 0.5 dB in Z_{DR}. If we use Z_{DR} values 0.5 dB less than the observed value, the D_0 decreases by about 0.3~0.5 mm and the N_0 increases by several to ten times. For example, the D_0 varied from 1.5 to 3.5 mm and the N_0 varied from 2 to 20 at 1005JST, while the D_0 varied from 2.0 to 3.7 mm and the N_0 varied from 1 to 6 using the observation value. Even if the observed value contains some system bias, the DSD of 1005JST echo has still large D_0 and small No. On the DSD above 2 km of the 1013JST echo, the new D_0 varies from 0.7 to 1 mm and the N_0 varies from 10^4 to 2×10^5, while the D_0 varies from 1.1 to 1.4 mm and the N_0 varies from 10^3 to 10^4 using the observation value. Since only 0.5 dB difference of Z_{DR} can change the DSD (or rainfall intensity) largely, accurate radar measurement is needed for accurate rainfall estimation and DSD estimation. Another parameter should be used to estimate the rainfall intensity such as K_{DP} as a next step.

5. Concluding remarks

In this study, using dual-polarization Doppler radar, the development process of an isolated echo is described from cloud physical and kinematic viewpoints. The polarimetric parameters of Z_H, Z_{DR}, and ZDP, are utilized in order to distinguish the ice region from the rain region and to infer the DSD of the rain region assuming an exponential DSD. Doppler velocity data was utilized in order to infer the in-cloud circulation. In this case study, the data from three RHI scans (early developing stage, rapid developing stage, and mature to decaying stage) were analyzed using both polarimetric data and Doppler velocity data. Table 2 briefly summarize the characteristics of DSD, Doppler velocity field, and $Z_H{}^i$ for each stage.

In the early stage, the echo developed by updraft. The polarimetric parameters indicated that a large Z_{DR} occupied the echo indicating a DSD of large D_0 and small N_0 but no ice signature was found at this stage. This characteristic suggested that these raindrops might form through the warm rain (collision and coalescence) process.

At the rapid development stage, a large Z_{DR} remained only at lower altitude

(<2 km), with a relatively small Z_{DR} above it. An ice signature was found above 3 km (environmental melting level). This result indicated that different types of DSD existed below the melting level. The DSD below 2 km was almost the same DSD as the early stage and the DSD above 2 km was much smaller D_0 and larger N_0. The Doppler velocity field indicated that the upper level raindrops (>2 km) are sustained by updraft, then only large raindrops appeared below it.

At the mature to decaying stage, a downdraft appeared at lower altitudes but updraft still existed above 2 km and anvil cloud appeared at the echo top (~8 km). The large Z_{DR} region dissipated and the ice signature was similar to that of the previous stage. At this stage, the calculated DSD was close to the DSD which was seen above 2 km in the previous stage.

In this case study, one noteworthy point is that quite different DSD appeared through its life cycle. One type of DSD had large D_0 and small N_0, and the other had small D_0 and large N_0. During the rapid development stage, both types of DSD coexisted. One inference for the reason is that this difference relates to the in-cloud circulation in the echo (distribution of updraft and downdraft). Although we do not have any independent in situ data for verification, the cloud physical results and the Doppler analysis suggest that our interpretation of the cloud development process is plausible. This study showed that combination of polarimetric and Doppler observation is useful for inferring changes in DSD according to the cloud development. We described changes of DSD corresponding to the echo development by using only Z_{DR}, ZDP, and Doppler velocity data. For further study of cloud physics with remote sensing procedure, observations adding other polarimetric parameters such as K_{DR} and ρ_{hv} are expected.

Acknowledgments

The authors express their thanks to the members of the Meteorological Laboratory, Graduate School of Science, Hokkaido University, for helping with the radar observation. This study was partly supported by Grant-in-Aid (No. 03554011) of the Ministry of Education, Science and Culture of Japan.

References

Balakrishnan, N. and D.S. Zrnic', 1990. Estimation of rain and hail rates in mixed-phase precipitation. J. Atmos. Sci., **47**, 565-583.

Conway, J.W. and D.S. Zrnic', 1993. A study of embryo production and hail growth using

dual-Doppler and multiparameter radars. Mon. Wea. Rev., **121**, 2511-2528.
Doviak, R.J. and D.S. Zrnic', 1984. Doppler radar and weather observations. Academic Press, 458 pp.
Golestani, Y., V. Chandrasekar and V.N. Bringi, 1989. Intercomparison of multiparameter radar measurements. Proc. 24th Conf. Radar Meteorology, Amer. Meteor. Soc., 309-314.
Hall, H.P.M., J.W.F. Goddard and S.M. Cherry, 1984. Identification of hydrometeors and other targets by dual-polarization radar. Radio Sci., **19**, 132-140.
Illingworth, A.J., 1992. A radar study of the formation of rain in convective clouds. Proc. 11th Int. Conf. Cloud and Precipitation, Montreal, 135-138.
Illingworth, A.J. and I.J. Caylor, 1989. Polarization radar estimation of raindrop size spectra and rainfall rates. J. Atmos. Ocean. Tech., **6**, 939-949.
Illingworth, A.J., J.W.F. Goddard and S.M. Cherry, 1987. Polarization radar studies of precipitation development in convective storms. Quart. J. Roy. Meteor. Soc., **113**, 469-489.
Meischner, P.F., V.N. Bringi, D. Heimann and H. Höller, 1991. A squall line in southern Germany : Kinematics and precipitation formation as deduced by advanced polarimetric and Doppler radar measurements. Mon. Wea. Rev., **119**, 678-701.
Pruppacher, H.R. and J.D. Beard, 1970. Microphysics of clouds and precipitation. D. Reidel Publishing Company, 714 pp.
Sachidananda, M. and D.S. Zrnic', 1987. Rain rate estimates from differential polarization measurements. J. Atmos. Oceanic Technol., **4**, 588-598.
Seliga, T.A. and V.N. Bringi, 1976. Potential use of radar differential reflectivity measurements at orthogonal polarizations for measuring precipitation. J. Appl. Meteor., **15**, 69-76.
Takahashi, T., K. Yoneyama and Y. Tsubota, 1989. Rain duration in Hawaiian trade-wind rainbands — Aircraft observation. J. Atmos. Sci., **46**, 937-955.
Uyeda, H., R. Shirooka, K. Iwanami, A. Takemoto and K. Kikuchi, 1990. Observation of vertical structure of convective snow clouds with a dual-polarization radar in Hokkaido, Japan. Proc. 25th Int. Conf. Radar Meteor., Paris, Amer. Meteor. Soc., 717-720.
Zrnic', D.S., 1991. Complete polarimetric and Doppler measurements with a singe receiver radar. J. Atmos. and Oceanic Technol., 8, 159-165.
Zrnic', D.S., N. Balakrishnan, C.L. Ziegler, V.N. Bringi, K. Aydin and T. Matejka, 1993a. Ploarimetric signatures in the stratiform region of a mesoscale convective system. J. Appl. Meteor., **32**, 678-693.
Zrnic', D.S., V.N. Bringi, N. Balakrishnan, K. Aydin, V. Chandrasekar and J. Hubbert, 1993b. Polarimetric measurements in a severe hailstorm. Mon. Wea. Rev., **121**, 2223-2228.